https://dx.doi.org/10.1016/j.scitotenv.2022.154788

Remarkable spring increase overwhelmed hard-earned autumn decrease in ozone pollution from 2005 to 2017 at a suburban site in Hong Kong, South China

Yangzong Zeren[1], Hai Guo[1*], Xiaopu Lyu[1], Beining Zhou[1], Xufei Liu[1], Leifeng Yang[2], Zibing Yuan[3], Yu Wang[1, 4]

[1] Air Quality Studies, Department of Civil and Environmental Engineering, Hong Kong Polytechnic University, Hong Kong, China

[2] South China Institute of Environmental Sciences, Ministry of Ecology and Environment, Guangzhou 510655, China

[3] School of Environment and Energy, South China University of Technology, Guangzhou 510006, China

[4] Institute for Environmental and Climate Research, Jinan University, Guangzhou 511443, China

*Corresponding author: ceguohai@polyu.edu.hk

Abstract

Ozone (O_3) pollution has been a persistent problem in Hong Kong, particularly in autumn when severe O_3 pollution events are often observed. In this study, linear regression analyses of long-term O_3 data in suburban Hong Kong revealed that the variation of autumn O_3 obviously leveled off during 2005–2017, mainly due to the significant decrease of autumn O_3 in 2013–2017 (period II), despite the increase in 2005–2012 (period I). In addition, the rise of O_3 in summer and winter also ceased since 2013. In contrary, O_3 continuously increased throughout the spring of 2005–2017, especially in period II. Consequently, an incessant increase of overall O_3 was observed during 2005–2017. A statistical model combining Kolmogorov-Zurbenko filter with multiple linear regressions, and a photochemical box model incorporating CB05

mechanism were applied to probe the causes of the above trends. In general, O_3 production was controlled by VOC-limited regime throughout 13 years. The meteorological variability and regional transport facilitated the O_3 growth in period I. In contrast, the unchanged O_3 level in period II was attributable to the negative impact of meteorological variability and reduction of regional transport effect on O_3 formation and accumulation, as well as the negligible change in locally-produced O_3. In autumn of period II, the inhibitory meteorological variability, reduced regional transport, and alleviated local production were the driving force for the hard-earned decrease of O_3. However, the remarkable rise of spring O_3 was caused by the reduction of NO_x, especially in the spring of period II. The findings of the long-term and seasonal variations of O_3 pollution in Hong Kong are helpful for future O_3 mitigation.

Keywords: Ozone pollution; Long-term trends; Local formation; Meteorological variability impact; Regional transport.

1 Introduction

Ground-level ozone (O_3) is the main component of photochemical smog, formed through complicated reactions among nitrogen oxides (NO_x), volatile organic compounds (VOCs), carbon monoxide (CO), and methane under sunlight (Atkinson, 2000). Stratosphere-troposphere exchange and special meteorological conditions that enhance dynamic transport and emissions of O_3 precursors also have an impact on surface O_3 levels (Collins et al., 2003; Cooper et al., 2004; Monks et al., 2015). Ground-level O_3 adversely affect human health, crop yields, vegetation growth, and biodiversity (Brauer et al., 2016; Agathokleous et al., 2020). In addition, O_3 is a greenhouse gas affecting climate change (Shindell et al., 2013). Over the years, O_3 pollution has deteriorated severely, causing many environmental problems (Fishman et al., 2003; Vingarzan, 2004; Young et al., 2013). Numerous studies have been conducted to elaborate the variations of tropospheric O_3 and the underlying causes from global to regional scales (Chang et al., 2017; Gaudel et al., 2018; Wang et al., 2019a; Lin et al., 2020). Continuous

increase of O_3 was witnessed in the United States and European countries in the last century (Derwent et al., 1996; Oltmans et al., 2006), whereas the decreases of upper-level O_3 and rural O_3 concentrations in recent years were due to the effective control of O_3 precursors (Simon et al., 2015; Yan et al., 2018; Georgoulias et al., 2019; Sicard, 2021). Unfortunately, due to the enhanced anthropogenic emissions, O_3 in most Asian countries is still increasing rapidly (Cooper et al., 2014; Seo et al., 2014; Akimoto et al., 2015; Kim & Lee, 2018).

The O_3 production is either in VOCs-limited or NO_x-limited or transitional regime depending on the levels of VOCs and NO_x and their ratios (Derwent et al., 2003). The O_3 production in urban and suburban areas of China is generally in VOCs-limited regime (Li et al., 2019), where the O_3 production decreases with the reduction of VOCs emissions while cutting NO_x level exhibits a counterproductive effect. In contrast, the O_3 production in rural areas of China is limited by NO_x (Wang et al., 2019b). As such, the rise of O_3 is considered an intractable and long-standing problem in China due to the diverse regimes of O_3 production over the vast territory which make the formulation and implementation of control strategies difficult. For example, the regional background O_3 in North China Plain (NCP) increased by 1.13 ± 0.01 ppbv/yr from 2003 to 2015, which resulted from the elevated VOCs emissions in this region (Ma et al., 2016), while a reduction in NO_x was found to cause an increasing O_3 with a rate of 0.8 – 1.3 ppbv/yr from 2006 to 2015 in East China (Xu et al., 2019). Regional transport and local production also exerted crucial impacts on O_3 variability in Pearl River Delta (PRD) region of South China, which caused an upward trend by 0.56 ppbv/yr from 2007 to 2017 (Yang et al., 2019). Since the launch of the "Clean Air Action" in 2013 with the goal of improving air quality in China, the concentration of fine particles ($PM_{2.5}$) has been successfully reduced, while O_3 pollution has unexpectedly increased significantly at a rate of 2.4 ppbv/yr from 2013 to 2019 (Lu et al., 2020). Multiple factors including little reduction in VOCs emissions, reduced NO_x in VOC-limited regime, and slowdown uptake of reactive gases in

74 particles, may account for this undesirable phenomenon (Zheng et al., 2018; Li et al., 2019;
75 Liu & Wang, 2020a). Interestingly, despite the rapid increase in O_3 levels in the adjacent
76 mainland China during the same period, the O_3 concentration in Hong Kong in autumn of
77 2013–2016 declined (Liu et al., 2019).

78 As an international metropolis, Hong Kong has been experiencing severe photochemical
79 pollution for decades. An increase of long-term vertical O_3 level within the planetary boundary
80 layer was recorded (Liao et al., 2021), so was the surface O_3 in suburban and background areas
81 (Wang et al., 2017; Wang et al., 2019a). Basically, the elevated O_3 is closely related to weather
82 conditions (*e.g.*, typhoons, continental anticyclone, low pressure troughs, and cold fronts) and
83 mesoscale circulations, which favor O_3 formation and accumulation (Huang et al., 2005, 2006;
84 Zeren et al., 2019). In view of the short distance between Hong Kong and the PRD region, the
85 polluted plumes from cities in the PRD may also aggravate O_3 pollution in Hong Kong. Apart
86 from the aforementioned factors, the role of anthropogenic and biogenic emissions of O_3
87 precursors in modulating O_3 concentration is vital (Cheng et al., 2013; Ling & Guo, 2014). In
88 the past decade, Hong Kong government devoted great efforts and developed manifold control
89 programs to alleviate O_3 pollution (Table S1), *i.e.*, stepwise phasing out diesel commercial
90 vehicles, regulating VOCs emissions from solvent usage, upgrading catalytic converters in
91 vehicles powered by liquified petroleum gas, and joint controls with Guangdong and Macau
92 governments. These measures led to hard-earned and successful reduction of ground-level O_3,
93 which has been confirmed by previous studies with the intimate relationship between the
94 diminished VOCs emissions and the reduction of O_3 (Xue et al., 2014; Lyu et al., 2016, 2017;
95 Wang et al., 2017). In addition, the regionally-transported O_3 in Hong Kong was also confirmed
96 to be leveling-off during autumn of 2013-2016 (Liu et al., 2019). However, most of the studies
97 focused on the O_3 formation from a chemical perspective, and the meteorological effects were
98 merely unveiled on high O_3 episode days. To our knowledge, the influence of meteorological

variability on the long-term variations of surface O_3 level in Hong Kong is still vaguely interpreted. Although the O_3 variations in the autumn after 2013 and their underlying causes were discussed (Liu et al., 2019), a comprehensive analysis of long-term and seasonal variations of O_3 levels in the post-2013 period is necessary, because since 2013, the implementation of rigorous air quality control measures in China has strongly affected the regional atmospheric chemistry due to the changes in chemical compositions. Such changes will also influence the air quality in Hong Kong through modulating the regional transport of O_3 and its precursors from PRD and eastern China. Furthermore, previous studies investigated the O_3 variations mainly in autumn (Xue et al., 2014; Liu et al., 2019), while few paid attention to the variability of O_3 in spring. Although Wang et al. (2017) noticed remarkable increase of spring O_3 in 2005-2014 in Hong Kong, the underlying causes were not fully explored.

Therefore, the long-term and seasonal variations of surface O_3 from 2005 to 2017 in Hong Kong were examined by analyzing the continuing observation data. In addition, the O_3 variation in the pre-2013 was re-examined and compared to that in the post-2013. The quantitative influence of meteorological variability on the O_3 trends was investigated through a statistical calculation combining Kolmogorov-Zurbenko filter with multiple linear regressions. The effects of changes in the level of photochemical precursors, and the contribution of regional transport were revealed with the aid of a photochemical box model. Overall, this study is expected to provide new insights into the multiple driving factors responsible for the long-term O_3 trend in the cities of South China, and potentially promote control strategies to mitigate O_3 in the future.

2 Methodology

2.1 Sampling site and data collection

Hong Kong is located on the southern coast of China (Figure 1a), where the subtropical maritime monsoon climate dominates. It is close to many other highly developed cities, *i.e.*,

Guangzhou, Dongguan, Shenzhen, Foshan, Zhongshan, Zhuhai and Macau, where extensive anthropogenic emissions occur. Severe O_3 pollution in Hong Kong is confirmed to partly originate from adjacent waters, including the Pearl River Estuary and the offshore waters of the South China Sea (Wang et al., 2018a; Zeren et al., 2019). Overall, not only the air pollutants transported from mainland cities but also the polluted plumes received from nearby waters pose a great threat to the air quality in Hong Kong. In this study, data was collected at Tung Chung (TC, Figure 1b), which is a suburban site and locates in a new town area in western Hong Kong. Apart from local emissions, this site can receive not only air plumes from upwind urban areas and the adjacent PRD region, but also air masses from Pearl River Estuary and the South China Sea, making it an ideal and representative site for the investigation of long-term variations of local and regional photochemical pollution in this coastal city of South China.

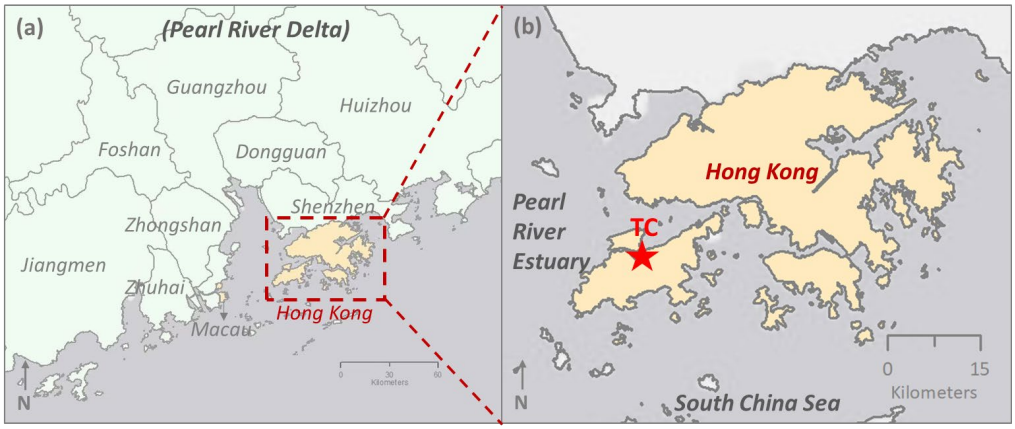

Figure 1. Geographic location of sampling site and its surrounding environments.

Air pollutants *i.e.*, O_3, NO_x, CO, SO_2 and VOCs were measured from 2005 to 2017 at TC using online instruments by the Hong Kong Environmental Protection Department (HKEPD). The detailed information regarding instrument types, techniques, detection limits, and time resolution can be found in Table S2. The hourly values were adopted in this study, and the data validated percentage for above species ranged from 83% to 97%. Specifically, the online GC-FID analyzer detected 29 VOC species involving 10 alkanes, 10 alkenes, and 9 aromatics

(Table S3). Calibration of the gas analyzers, certificated by Hong Kong Laboratory Accreditation Scheme (https://www.aqhi.gov.hk/gt/monitoring-network/air-quality-monitoring-network.html), was conducted on a regular basis. In addition, a weekly calibration using standard gases and built-in computerized programs (*e.g.*, auto-linearization and autocalibration) was operated to guarantee the credibility of the VOCs data. The strict quality assurance and quality control (QA/QC) procedures were followed throughout the sampling periods, and the details can be found in our previous studies (Ou et al., 2015; Wang et al., 2017). Table S4 lists the data capture rates of VOCs species during 2005-2017, generally ranging from 65% to 92%, except for that of trans-2-Pentene (0.51%), mainly due to its low concentration which was always under the low detection limit of instrument. In addition, the regular comparison between online measured VOCs concentrations and the whole-air canister collected VOCs concentrations analyzed by the University of California, Irvine (UCI) showed good agreement for alkanes (e.g., R^2 = 0.93 and 0.80, slope = 0.95 and 0.89 for propane and n-butane, respectively). Besides, the agreements for more reactive alkenes and aromatics were also reasonable (e.g., R^2 = 0.69 and 0.88, slope = 0.82 and 0.80 for propene and toluene, respectively). Apart from the chemical datasets, meteorological parameters including temperature (Temp), relative humidity (RH), solar radiation (SR), wind speed (WS), and direction (WD) were continuously monitored at the Hong Kong International Airport, about 3 km away from TC, and the planetary boundary layer height (PBLH) was available from the hourly reanalysis data of European Centre for Medium-Range Weather Forecasts (EAR5 with resolution of 0.25°, https://www.ecmwf.int/).

2.2 Quantification of impact factors for O_3 variation

To quantify the driving force for the long-term O_3 variation, the multiple statistical calculations and model simulation were adopted. Figure 2 shows the diagram of methods implemented in this study.

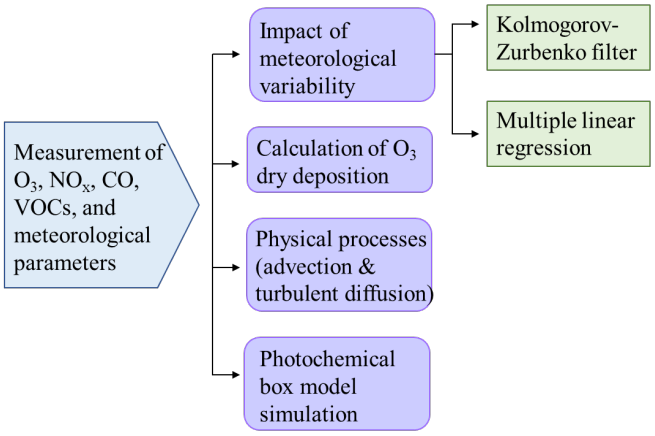

168

169 Figure 2. Flow diagram of methodology.

170 **2.2.1 Quantification of meteorological impact and physical processes**

171 To quantify the impact of meteorology on the ground-level O_3, a statistical calculation
172 combining Kolmogorov-Zurbenko (KZ) filter and stepwise multiple linear regression (MLR)
173 was implemented in this study. KZ filter is a moving average method to preserve the low-pass
174 signal processed by repeating iterations (Formula 1, Rao & Zurbenko, 1994):

175 $$Y_i = \frac{1}{m}\sum_{j=-k}^{k} A_{i+j} \quad \text{(Formula 1)}$$

176 where k represents the number of variables included on each side of target values, and the
177 moving window length is calculated as m = 2k + 1. A_{i+j} and Y_i denote the time series of input
178 and output, respectively. i is the time interval, and j stands for the number of windows. The
179 output of i^{th} pass turns to be the input of $(i+1)^{th}$ pass. KZ (m, n) indicates the filter calculated
180 through n iterations with a window length of m, aiming to remove the fluctuations higher than
181 period of $m \times n^{1/2}$ (days). Previous studies applied filters of KZ (15, 5) and KZ (365, 3) to
182 separate the observed O_3 (O(t), Formula 2) into three time-scale components (Rao et al. 1997;
183 Ma et al., 2016; Yang et al., 2019).

184 $$O(t) = W(t) + S(t) + L(t) \quad \text{(Formula 2)}$$

$$L(t) + S(t) = KZ\ (15,\ 5) = B(t) \quad \text{(Formula 3)}$$

$$W(t) = O(t) - KZ(15,\ 5) \quad \text{(Formula 4)}$$

$$L(t) = KZ(365,\ 3) \quad \text{(Formula 5)}$$

$$S(t) = KZ(15,\ 5) - KZ(365,\ 3) \quad \text{(Formula 6)}$$

where O(t) is the timeseries of observed daily maximum 8-hour average (DM8A) O_3 concentration. L(t) (Formula 5) and S(t) (Formula 6) refer to the long-term and seasonal components, respectively. W(t) (Formula 4) reflects the short-term variation calculated by mesoscale- and/or synoptic-scale factors. The sum of L(t) and S(t) is defined as the baseline (B(t)) (Formula 3) for convenience of the following calculations. The stepwise MLR was established between DM8A O_3 and the meteorological components in different time scales.

$$A_W(t) = \sum b_{W_i} \times M_{W_i} + c_W \quad \text{(Formula 7)}$$

$$A_B(t) = \sum b_{B_i} \times M_{B_i} + c_B \quad \text{(Formula 8)}$$

$$\varepsilon_W(t) = W(t) - A_W(t),\ \varepsilon_B(t) = B(t) - A_B(t) \quad \text{(Formula 9)}$$

$$\varepsilon(t) = \varepsilon_W(t) + \varepsilon_B(t) \quad \text{(Formula 10)}$$

$$A(t) = \varepsilon(t) + \sum b_{W_i} \times \bar{M}_{W_i} + \sum b_{B_i} \times \bar{M}_{B_i} + c_W + c_B \quad \text{(Formula 11)}$$

where $A_W(t)$ (Formula 7) and $A_B(t)$ (Formula 8) calculated by the multiple linear regressions are the short-term and baseline O_3 concentrations, respectively. M_{W_i} and M_{B_i} stand for the meteorological variables in the two-time scales. The variables incorporate daily maximum Temp, daily minimum RH, daytime (07:00-19:00 LST) average of SR, U & V wind components, and PBLH, which are acknowledged as the important factors affecting the ambient O_3 concentrations (Sanchez-Ccoyllo et al., 2006; Lee et al., 2014; He et al., 2017; Liu

& Wang, 2020b). b_{W_i} and b_{B_i} represent the regression coefficients, while c_W and c_B indicate the interceptions of regression formulas. The residuals between observations and calculations can be expressed by $\varepsilon(t)$ (Formula 10). In addition, a base condition related to the mean values of meteorological data on the same date throughout entire period ($\overline{M}$) was calculated to preserve the annual variation pattern. The O_3 concentration after ruling out the impact of meteorological variability can be determined by $A(t)$ (Formula 11), which is the sum of $\varepsilon(t)$ and base conditions. Moreover, the impact of each meteorological parameter was calculated by considering the individual meteorological variables in M_{W_i} and M_{B_i}. This calculation method has been proved valid in a previous work studying the O_3 variation in the PRD region (Yang et al., 2019).

In addition to the quantification of meteorological impact, the hourly O_3 dry deposition loss rate was estimated through Formula 12 (Luhar et al., 2017; Wang et al., 2018b):

$$O_3 \text{ dry deposition rate} = \int_0^t \frac{V_d}{PBLH} \times C_{O3} \quad \text{(Formula 12)}$$

where V_d represents O_3 dry deposition velocity, PBLH is planet boundary layer height, t stands for one hour, and C_{O3} depicts the hourly observed O_3 concentration. Since our sampling site locates in the suburban area, we applied 0.6 cm/s as the O_3 dry deposition velocity in this study (Zhang et al., 2003).

According to the continuity equation of O_3 budget at a given location (Text S1), the regionally-transported O_3 is attributed to the physical processes of advection and turbulent diffusion, which is part of the observed O_3, in addition to the effects of chemical production and loss and dry deposition. It is notable that this method might generate some negative values, which were corresponding to the dilution effect of regional transport.

2.2.2 Observation-based box model

A photochemical box model coupled with carbon bond mechanism (CB05) was employed to simulate local net O_3 formation (*i.e.*, O_3 production minus O_3 destruction) during 2005–2017. CB05 is a condensed mechanism developed by U.S. Environmental Protection Agency (EPA) (Yarwood et al., 2005). It can provide reasonable simulated results in chemical transport models such as WRF-Chem/CMAQ (Appel et al., 2007; Wang et al., 2015) and in-situ photochemical study (Wang et al. 2017). The hourly concentrations of NO, NO_2, CO, SO_2 and 29 species of VOCs observed at TC were adopted as the input data at each hour. The original VOC species for the lumped groups in the condensed mechanism are provided in Table S3. In addition, the photolysis rates of individual species were determined using the Tropospheric Ultraviolet and Visible Radiation model (TUV v5, Madronich & Flocke, 1997) on the basis of actual conditions of Hong Kong, such as location, meteorological conditions, and time period of sampling measurement. The model output included the values of radicals (*i.e.*, RO, RO_2, OH and HO_2), intermediates and O_3. The hour-to-hour simulation was carried out every day from 00:00 local standard time (LST) to 23:00 LST in 2005–2017, except those days with missing data of precursors (i.e., days with any 6 consecutive hours of missing VOCs data, and the data completeness lower than 75% during 07:00-19:00 LST). In total, the simulated results of 3801 days performed well with 80% validity for 4748 days (the total number of days throughout 13 years). The consecutive model running was independently conducted in each year, in which an additional running for the first month was operated as spin-up. The correlation coefficient (COE) (Rodgers & Nicewander, 1988), index of agreement (IOA) (Willmott, 1981), and root mean square error (RMSE) (Willmott, 1981) between simulations and observations were utilized to assess the simulation performance. The detailed calculation formulas and statistical meanings are described in Text S2. The main O_3 production and destruction pathways are presented in Text S3. Although the physical processes are not included in this model, our previous study has proven the good performance of the model on the simulation of photochemical reactions (Wang et al., 2017). In fact, the deficiency of the model in

consideration of atmospheric dynamics enables us to estimate the contribution of physical processes to O_3 concentration.

Apart from the simulation of O_3 concentration, the model also calculates the relative incremental reactivity (RIR) to identify the sensitivity of O_3 production to its precursors (Cheng et al., 2010; Xue et al., 2014; Wang et al., 2017). RIR is defined as the percentage change in daytime (07:00 – 19:00 LST) O_3 production per the percent change in O_3 precursors. The calculation equation of RIR is shown in Formula 13:

$$\mathrm{RIR}\ (X) = \frac{[P^{S}_{\mathrm{O3-NO}}(X) - P^{S}_{\mathrm{O3-NO}}(X-\Delta X)]/P^{S}_{\mathrm{O3-NO}}(X)}{\frac{\Delta S(X)}{S(X)}} \qquad \text{(Formula 13)}$$

where X stands for the specific O_3 precursors, *i.e.* NO_x, VOCs or CO. "S" denotes the sampling site. $S(X)$ is the measured concentration of X, and $\Delta S(X)$ is the hypothetical change of X concentration. We hypothesized 10% for $\Delta S(X)$ /$S(X)$ in this study. $P^{S}_{\mathrm{O3-NO}}(X)$ and $P^{S}_{\mathrm{O3-NO}}(X-\Delta X)$ represent the net O_3 production in base run and a scenario with the change of $\Delta S(X)$ in X species, respectively.

Moreover, to study the O_3 variation induced by the long-term changes of photochemical precursors, comparisons were made between the base simulation using the concentrations of all precursors and the scenario simulations with constrained NO_x, CO and VOCs concentrations, respectively. Specifically, the simulation based on measured concentrations of O_3 precursors was set as the base case. The constrained scenarios were implemented under the same model settings as those of the base case, except that one of the VOCs, NO_x and CO concentrations was maintained unchanged, *i.e.*, assuming no change for this specified precursor since 2005, respectively. The impacts of individual precursors during 2005–2017 were examined by the differences between the results of base case and scenario simulations. In addition, the model was re-processed with the constrained concentrations of VOCs, NO_x, and CO in 2013,

278 respectively, to exclusively study the impacts of the precursors on O_3 trend in period II. Overall,
279 six scenario experiments were conducted in this study, which are shown in Table S5.

280

281 **3 Results and discussion**

282 **3.1 Trends of observations**

283 **3.1.1 Long-term variations of O_3 and its precursors**

284 Figure 3 displays the temporal variations of O_3 and its precursors throughout the period of
285 2005–2017. The long-term trends were evaluated based on a linear regression of daily averages
286 (24-hour), where *p* value determined by t-test was used as a reference to indicate significant
287 level of changes. For a better visualization of the annual and seasonal trends, the datasets were
288 processed into monthly averages with 95% confidence intervals.

289 An increase in DM8A O_3 with a rate of 0.32 ± 0.07 ppbv/yr ($p < 0.01$) throughout 2005–2017
290 was observed, and the variation rate of daily average O_3 was 0.28 ± 0.05 ppbv/yr ($p < 0.01$) in
291 this period, indicating a long-term increase of O_3 pollution in Hong Kong. The elevation of O_3
292 levels was consistent with previous findings of the long-term O_3 variations in Hong Kong
293 (Table S6). However, this study found that the rising rate of O_3 at TC slowed down compared
294 to the upward trend in 2005–2014 with a rate of 0.56 ± 0.01 ppbv/yr (Wang et al., 2017). By
295 dividing the study period into two periods, it was discovered that the O_3 mainly increased
296 during 2005–2012 (defined as period I) at rates of 0.96 ± 0.15 ppbv/yr ($p < 0.01$) for DM8A
297 O_3 and 0.72 ± 0.09 ppbv/yr ($p < 0.01$) for daily average O_3, whereas these values leveled off in
298 2013–2017 (period II). The insignificant variations of DM8A O_3 ($p = 0.57$) and daily average
299 O_3 ($p = 0.12$) in period II revealed steady O_3 pollution at the suburban site in Hong Kong since
300 2013. A previous study even reported a decrease in O_3 mixing ratio in autumn of 2013-2016 at
301 the same site (Liu et al., 2019). Moreover, the number of high O_3 episode days (hourly

maximum O_3 concentration exceeding 100 ppbv) presented an increasing trend in period I with a rate of 1.6 day/yr ($p < 0.05$), while it insignificantly decreased at a rate of -1.2 days/yr ($p = 0.53$) in period II (Figure S1). This phenomenon was also validated by the increasing number of hours with O_3 concentration exceeding 160 μg/m^3 in period I (9.4 ± 3.2 hour/yr, $p < 0.05$) and an insignificant decrease of that in period II (-9.4 ± 10.9 hour/yr, $p = 0.45$) (Figure S2). These results confirmed that O_3 pollution in Hong Kong was alleviated from 2013 to 2017.

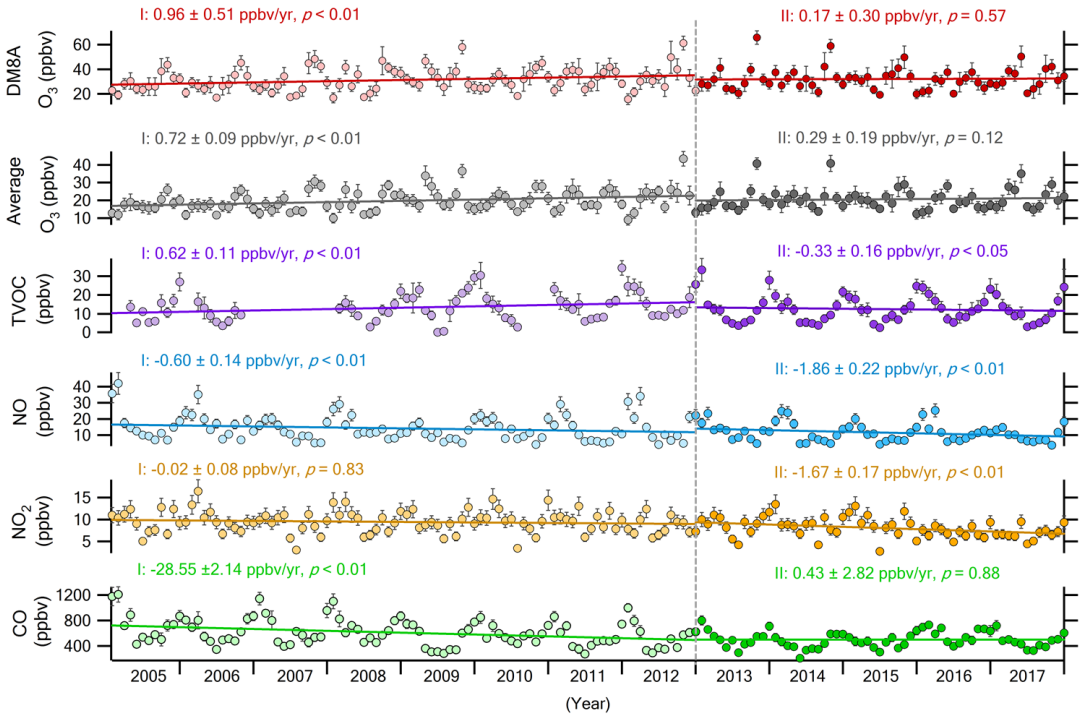

Figure 3. Variations of O_3 and its precursors from 2005 to 2017 (monthly averages are presented and error bars indicate 95% confidence intervals).

Contrary to the increase in O_3, a notable decline of NO was found at a rate of -0.71 ± 0.06 ppbv/yr ($p < 0.01$) during 2005–2017. This trend was also identified in period I (-0.60 ± 0.14 ppbv/yr, $p < 0.01$) and period II (-1.9 ± 0.22 ppbv/yr, $p < 0.01$). Weakened NO titration has been confirmed to be the main reason for the increase of O_3 in VOCs-limited regime (Wang et al., 2017; Wang et al., 2018b). Hence, it is plausible to infer that the NO reduction in Hong Kong might partly contribute to the elevation of O_3 concentration. Furthermore, the NO_2 levels

317 also decreased (-0.38 ± 0.05 ppbv/yr, $p < 0.01$) during 2005–2017, mainly attributable to the
318 decrease of NO_2 in period II at a rate of -1.7 ± 0.17 ppbv/yr ($p < 0.01$) despite no changes in
319 period I (-0.02 ± 0.08 ppbv/yr, $p = 0.83$). The reduced NO_2 decreased consumption of OH
320 radicals (Liu et al., 2019), which would enhance O_3 formation. Moreover, CO decreased at a
321 rate of -18 ± 0.92 ppbv/yr ($p < 0.01$) during 2005–2017, likely favorable to O_3 reduction.
322 Further examination found that the decline mainly occurred in period I (-29 ± 2.1 ppbv/yr, $p <$
323 0.01) compared to the constant trend in period II ($p = 0.88$). The reduction in CO was due to
324 the effective control of vehicle emissions in Hong Kong (Table S1) (Guo et al., 2007; Liu et
325 al., 2019), and industrial and on-road mobile sources in PRD (Zheng et al., 2009; Li et al.,
326 2017), which was also reported in other regions of China (Feng et al., 2020). The stable CO in
327 period II (0.43 ± 2.8 ppbv/yr, $p = 0.88$) might be affected by the long-range transport of CO
328 emitted from the biomass burning activities in Southeast Asian countries in recent years (Wang
329 et al., 2019a). Although the overall trend of TVOC (29 VOC species detected in this study)
330 was steady from 2005 to 2017 (-0.08 ± 0.05 ppbv/yr, $p = 0.12$), an increase with a rate of 0.64
331 ± 0.11 ppbv/yr ($p < 0.01$) was found in period I. Contrarily, a reduction (-0.33 ± 0.16 ppbv/yr,
332 $p < 0.05$) was observed in period II. However, the OH reactivity of TVOC (Text S4)
333 continuously increased from 2005 to 2017 (0.02 ± 0.01 s^{-1}/yr, Figure S3), indicating the
334 increasing contribution of TVOC to photochemical reactions (Yang et al., 2016), which
335 possibly resulted in the enhancement of local O_3 production. Further investigation on the OH
336 reactivity of TVOC in the two periods discovered an increase in period I (0.18 ± 0.12 s^{-1}/yr, p
337 < 0.01) but a stable pattern in period II (0.05 ± 0.04 s^{-1}/yr, $p = 0.08$), which suggested the
338 alleviation of VOCs after 2013. The declined TVOC and NO_x levels in period II were ascribed
339 to the control measures formulated and implemented by local government, *e.g.*, diminished
340 emissions from diesel commercial vehicles and replacement of catalytic converters in vehicles
341 fueled by liquified petroleum gas (Lyu et al., 2016, 2017). Since the O_3 formation at TC is
342 VOCs-limited (Wang et al., 2017; Liu et al., 2019), the growth of TVOC was one of the reasons

for the O_3 enhancement in period I. Instead, the decreased TVOC in period II was favorable for the reduction in O_3 production. Although previous work reported that the O_3 concentration in Hong Kong decreased in autumn of 2013-2016 (Liu et al., 2019), no decline of O_3 was observed throughout period II in this study. Thus, the seasonal O_3 variations were investigated as follows.

3.1.2 Seasonal variations of O_3 and its precursors

Figure 4 shows the seasonal variations (March–May, June–August, September–November, and December–February defined as spring, summer, autumn, and winter, respectively) of DM8A O_3 and O_3 precursors from 2005 to 2017. It is notable that the rising trend of O_3 in spring (0.62 ± 0.13 ppbv/yr, $p < 0.01$) was the most obvious in the four seasons. The springtime increase occurred not only in period I (1.4 ± 0.27 ppbv/yr, $p < 0.01$) but also in period II with a more rapid rate (1.8 ± 0.48 ppbv/yr, $p < 0.01$). The overall O_3 trend in summer was 0.40 ± 0.15 ppbv/yr ($p < 0.01$), while it was 1.6 ± 0.32 ppbv/yr ($p < 0.01$) in period I, and insignificant (-0.78 ± 0.59 ppbv/yr, $p = 0.19$) in period II. A moderate increase was found in winter (0.24 ± 0.10 ppbv/yr, $p < 0.05$), despite no significant variation in both period Iand period II. Strikingly, the autumn O_3 variation leveled off in 2005–2017 (-0.21 ± 0.16 ppbv/yr, $p = 0.20$), which was obviously different from the increasing pattern in 2005–2014 (0.67 ± 0.07 ppbv/yr, Wang et al., 2017). Further investigation revealed that the autumn O_3 increased in period I at a rate of 0.60 ± 0.27 ppbv/yr ($p < 0.05$), while it remarkably decreased in period II at a rate of -2.0 ± 0.64 ppbv/yr ($p < 0.01$), in agreement with the variation rate calculated using hourly O_3 values during the same period (-2.02 ± 0.003 ppbv/yr, Liu et al., 2019). The obvious increase of spring O_3 (2.2 ± 0.39 ppbv/yr, $p < 0.01$) and the decrease of autumn O_3 (-2.0 ± 0.44 ppbv/yr, $p < 0.01$) were also found in the daily average (24-hour) O_3 variations during this period (Figure S4). The sharp decrease of autumn O_3 in period II led to the overall leveling-off of autumn O_3 during 2005–2017. The reason for the alleviated O_3 pollution in autumn might be due to the levelled-

off regional transport of O_3 and the mitigation of locally-formed O_3 in autumn in Hong Kong during 2013-2016 (Liu et al., 2019).

Overall, the O_3 variations in both spring and autumn in period I presented increasing trends, while the hard-earned O_3 decrease in autumn was offset by the remarkable increase of spring O_3 in period II, leading to an overall unchanged O_3 variation in this period. The underlying causes for the seasonal variations were thoroughly discussed in the following sections.

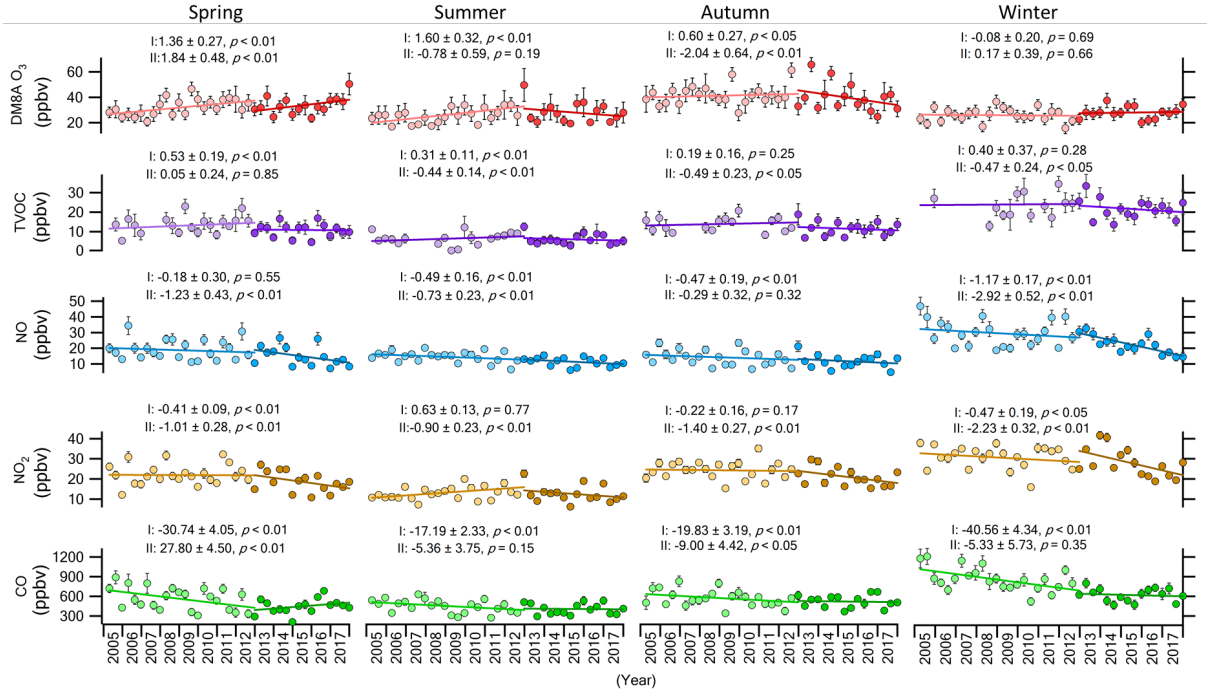

Figure 4. Seasonal variations of DM8A O_3 and O_3 precursors during 2005–2017 (data points are integrated into monthly averages and 95% confidence intervals are presented as error bars).

Consistent with the overall trend of NO during 2005–2017, a decrease ($p < 0.01$) of NO was discovered at rates of -0.54 ± 0.22 ppbv/yr, -0.52 ± 0.07 ppbv/yr, -0.45 ± 0.08 ppbv/yr and -1.2 ± 0.17 ppbv/yr in spring, summer, autumn, and winter, respectively. Furthermore, the NO decrease in spring (-1.2 ± 0.43 ppbv/yr, $p < 0.01$), summer (-0.73 ± 0.23 ppbv/yr, $p < 0.01$) and winter (-2.9 ± 0.52 ppbv/yr, $p < 0.01$) in period II was greater than that in period I with statistical significance ($p < 0.05$), implying that the titration of NO in period II was weakened,

which might subsequently facilitate the increase of O_3. Note: despite decreased autumn NO in period I, it remained stable in period II (p = 0.32). Analogously, NO_2 in spring, autumn and winter decreased at rates of -0.41 ± 0.09 ppbv/yr (p < 0.01), -0.52 ± 0.08 ppbv/yr (p < 0.01) and -0.55 ± 0.09 ppbv/yr (p < 0.01), respectively. Same as NO, the NO_2 reduction in period II were more prompt than that in period I, probably causing increased O_3 formation to some extent due to decreased consumption of OH radicals by NO_2. In addition, the TVOC levels remained stable (p > 0.05) in spring and summer, but decreased in autumn and winter with rates of -0.33 ± 0.07 ppbv/yr (p < 0.01) and -0.31 ± 0.13 ppbv/yr (p < 0.05), respectively. Specifically, the reduction of TVOC in these two seasons was mainly associated with the decrease of TVOC in period II (p < 0.05), leading to the overall decrease of O_3 formation in autumn and winter because of the VOC-limited regime at TC. The reduced TVOC was attributable to aforementioned control measures implemented by Hong Kong government. It could also benefit from the alleviation of background pollution in PRD region because of the reduction in VOCs emissions since 2014 from Guangdong province (Figure S5), the upwind region of Hong Kong in autumn and winter under winter monsoon (Jiang et al., 2010). Furthermore, the decreases (p < 0.01) of CO in all seasons (-17 ± 1.7 ppbv/yr, -9.4 ± 1.1 ppbv/yr, -11 ± 1.4 ppbv/yr, and -35 ± 1.9 ppbv/yr in spring, summer, autumn and winter, respectively) reduced the O_3 formation due to the positive contribution of CO to O_3. In contrast, CO exclusively increased in spring of period II (20 ± 5.1 ppbv/yr, p < 0.01). Apart from emissions of local vehicles, the long-range transport of CO emitted from biomass burning in Southeast Asia might also be one of the reasons for the striking increase of CO in spring of period II, because of the extensive biomass burning activities in springtime over Indochina Peninsula (Xue et al., 2020; Liao et al., 2021).

3.1.3 Temporal variations of meteorological parameters

Meteorological conditions are also closely related to the O_3 formation, accumulation, and transport. The annual and seasonal variations of meteorological conditions during 2005–2017 are summarized in Table S7. Slow increase of temperature (0.09 ± 0.02 °C/yr, $p < 0.01$) and solar radiation (SR, 0.06 ± 0.03 MJ m^{-2}/yr, $p < 0.05$) as well as slight decrease of WS (-0.02 ± 0.01 m s^{-1}/yr, $p < 0.01$) were seen, favorable to the O_3 formation and accumulation from 2005 to 2017. However, above changes in temperature, SR and WS were not completely consistent in each sub-period. Compared to the overall trend, the reduction of WS (-0.01 ± 0.01 m s^{-1}/yr, $p = 0.32$) was insignificant in period I. Nevertheless, a much stronger enhancement of SR (0.16 ± 0.05 MJ m^{-2}/yr, $p < 0.01$) was unveiled during this period, which is beneficial to the O_3 formation. The increase of SR in period I was possibly caused by the sharp reduction of particular matter over PRD region during this period (Lin et al., 2018). In period II, the rise of temperature (0.35 ± 0.10°C/yr, $p < 0.01$) and decline of WS (-0.07 ± 0.02 m s^{-1}/yr, $p < 0.01$) likely led to O_3 increase, whereas the growth of PBLH (6.3 ± 2.5 m/yr, $p < 0.05$) tended to reduce O_3 (Ding et al., 2004; Haman et al., 2014). Seasonally, the meteorological conditions in summer were more favorable to the formation of O_3, because of the increases in temperature (0.10 ± 0.01 °C/yr, $p < 0.01$), SR (0.15 ± 0.06 MJ m^{-2}/yr, $p < 0.01$) as well as the decrease of RH (-0.23 ± 0.07 %/yr, $p < 0.01$) and WS (-0.05 ± 0.01 m s^{-1}/yr, $p < 0.01$). These phenomena were not found in other seasons except for a slight increase in temperature in spring (0.07 ± 0.03 °C/yr, $p < 0.05$).

3.2 Quantitative impact of meteorological variability

The variations of O_3 induced by meteorological variability (ΔDM8A O_3, $O(t)$ - $A(t)$) are demonstrated in Figure 5a. Overall, the impact of meteorological variability on the long-term O_3 trend at TC was insignificant ($p = 0.93$). Furthermore, a slight increase of ΔDM8A O_3 level at 0.12 ± 0.06 ppbv/yr ($p < 0.1$) was found in period I, whereas an obvious decreasing trend at a rate of -0.25 ± 0.12 ppbv/y ($p < 0.05$) was observed in period II. These results indicated that

the meteorological variability could result in an increase in O_3 concentration in period I, and a decrease in period II. The impacts of individual meteorological parameters are summarized in Table S8. The enhancement of O_3 in period I was probably attributed to SR, indicated by the increase of the observed SR (0.08 ± 0.03 ppbv/yr, $p < 0.05$). The U and V winds (0.13 ± 0.02 ppbv/yr, $p < 0.01$ for U wind; 0.03 ± 0.005 ppbv/yr, $p < 0.01$ for V wind) also made positive contributions though their effects were unable to be directly inferred from the observed wind speeds in Section 3.1. Although the V wind favored the O_3 accumulation in period II (0.05 ± 0.01 ppbv/yr, $p < 0.01$), the U wind and PBLH overwhelmed its effect and resulted in a noticeable reduction of O_3 (-0.19 ± 0.03 ppbv/yr, $p < 0.01$ and -0.34 ± 0.05 ppbv/yr, $p < 0.01$, respectively). The influence of PBLH was in line with its increasing trend since 2013 (Section 3.1).

Figure 5b presents the seasonal ΔDM8A O_3 variations. The meteorological variability led to the increase of O_3 levels in summer and winter with rates of 0.18 ± 0.05 ppbv/yr, ($p < 0.01$) and 0.14 ± 0.07 ppbv/yr ($p < 0.05$), respectively, consistent with the discovery of Lam et al. (2018), who reported that the summer O_3 transported from PRD region increased at 0.2 ppbv/yr in last decade due to the increase in the effect of tropical cyclones in West Pacific Ocean. Similar to the analysis in Section 3.1, the meteorological parameters including Temp, RH, SR, U wind, and V wind effectively accelerated O_3 formation and accumulation in summer (Table S8), while the increase of winter O_3 was mainly attributed to the U wind, which might be related to the contribution of aged air masses transported from East China Sea under northeasterly wind (Wang et al., 2018). In contrast, the O_3 level in autumn was decreased due to meteorological variability at a rate of -0.14 ± 0.10 ppbv/yr ($p < 0.05$), which was mainly related to the decreasing trend in period II (-0.65 ± 0.24 ppbv/yr, $p < 0.01$), revealing that the reduction of autumn O_3 partially benefited from the meteorological variability. It was also confirmed by Liu et al. (2019) that the weather conditions in the autumns of 2013–2016 could restrain the O_3

accumulation in Hong Kong. This study further discovered that RH, U wind and PBLH were the main driving factors for the impact of meteorology on the inhabitation of autumn O_3 after 2013 (Table S8). In addition, the impact of meteorology on spring O_3 during 2005–2017 was insignificant ($p = 0.53$), despite an increasing effect in period I (0.60 ± 0.13 ppbv/yr, $p < 0.01$) but no significant impact on period II ($p = 0.25$).

Figure S6 displays long-term and seasonal O_3 variations after ruling out the impact of meteorological variability. It is notable that the O_3 variation during 2005-2017 presented the same trend as that of observation data (0.32 ± 0.07 ppbv/yr, $p < 0.01$). Comparably, the spring DM8A O_3 also increased with a rate of 0.69 ± 0.11 ppbv/yr ($p < 0.01$) after ruling out the impact of meteorological variability. The results indicated that the O_3 increase, especially the sharp increase of spring O_3, was likely attributable to other factors. Therefore, the following sections will further analyze the physical and chemical factors responsible for the long-term and seasonal O_3 variations.

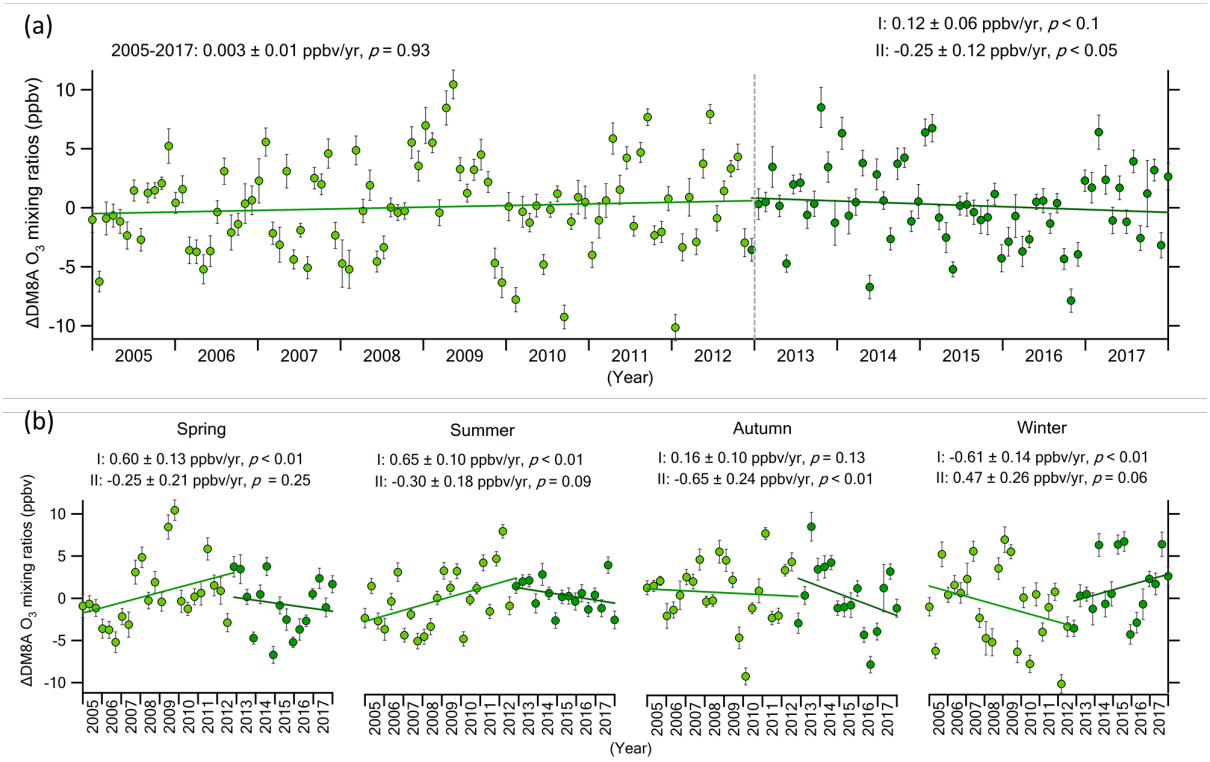

Figure 5. (a) Annual and (b) seasonal variations of O_3 induced by meteorological variability (ΔDM8A O_3) during 2005–2017 (data are integrated into monthly averages, and 95% confidence intervals are shown as error bars).

3.3 Quantitative contributions of physical and chemical processes

3.3.1 Impacts of physical processes

The annual and seasonal variations of dry deposition loss rate are shown in Figure S7. The average O_3 dry deposition loss rate was 1.1 ± 0.02 ppbv/hr during 2005-2017, and the mean values in spring, summer, autumn and winter were 1.3 ± 0.05 ppbv/hr, 0.92 ± 0.05 ppbv/hr, 1.2 ± 0.05 ppbv/hr, and 0.86 ± 0.04 ppbv/hr, respectively. These values are lower than that (2.8 ± 0.3 ppbv/hr) at TC simulated by a WRF-Chem model in our previous study (Zeren et al., 2019), mainly because only high O_3 episode days were considered in the previous study. The dry deposition of O_3 would enhance with the increase of ambient O_3 concentration. Overall, the dry deposition loss rates in this study are within a reasonable level.

Moreover, the chemical production and destruction of O_3 at TC was simulated using a photochemical box model. To assess the model simulation performance on photochemistry, the monthly average diurnal patterns (07:00–19:00 LST) of simulated and observed O_3 from 2005 to 2017 are shown in Figure 6. In general, the model well reproduced the variations of observed O_3 concentrations in terms of diurnal and seasonal characteristics. The O_3 variations affected by the dynamic processes such as horizontal, vertical advections, turbulent diffusions and dry deposition were not considered in this model. Thus, the overall (00:00–23:00 LST) simulated average (17 ± 0.56 ppbv) was slightly lower than the observed value (23 ± 0.48 ppbv). The model performance was evaluated based on the values of IOA, COE and RMSE for each year (Table S9). Specifically, the values of IOA ranged from 0.78 to 0.90, indicating the simulated results were acceptable. The IOA range was comparable to the previous studies (0.71–0.89,

Lyu et al., 2017; Wang et al., 2017). Furthermore, the simulated and observed values showed a good correlation indicated by the high values of COE (0.73–0.91). Besides, the range of RMSE (11–16) was within the reasonable range in comparison with previous work (10-24, Zhang & Dubey, 2009; Wang et al., 2019b). In spite of the good performance of model simulation, better agreement between simulation and observation was found in the upper-level O_3 than that in the lower-level O_3 concentrations, because the model excludes the background and regionally-transported O_3, which account for higher percentage in the lower-level O_3 concentrations.

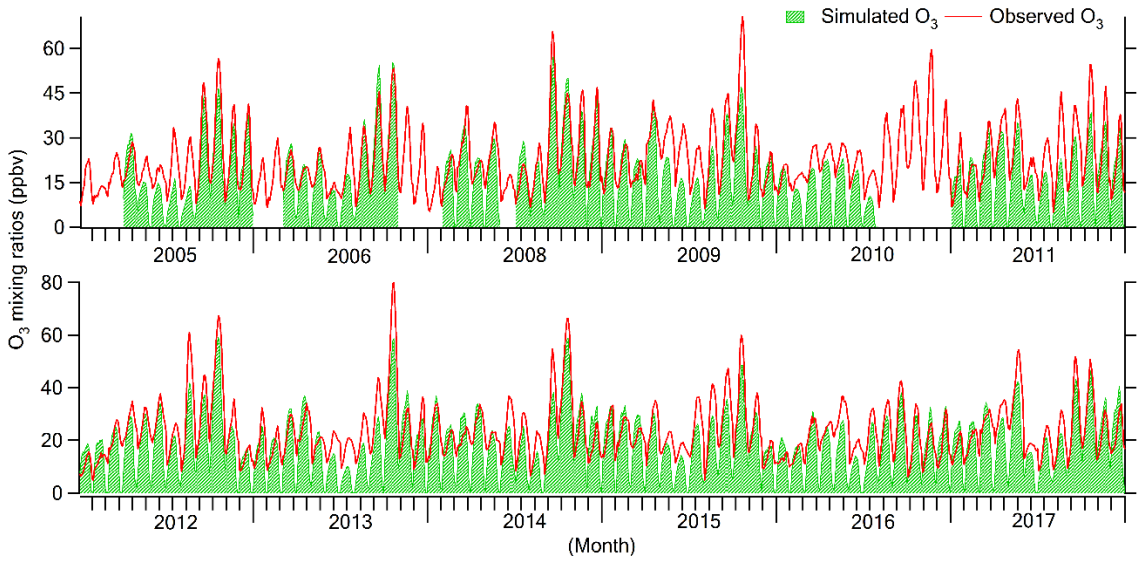

Figure 6. Monthly average diurnal patterns (07:00–19:00 LST) of simulated and observed O_3 from 2005 to 2017 (the missing data in 2007 and other vacant periods in simulated O_3 are due to the unavailable VOCs data during instrument maintenance).

Figure 7 presents the contribution of regional transport effect to O_3. The overall trend of regionally-transported O_3 remained stable (-0.04 ± 0.05 ppbv/yr, p = 0.38) in 2005–2017. Furthermore, the regionally-transported O_3 notably increased in period I with a rate of 0.34 ± 0.11 ppbv/yr (p < 0.01), consistent with the results reported in previous studies (Xue et al., 2014; Wang et al., 2017). However, a decline occurred with a rate of -0.33 ± 0.16 ppbv/yr (p <

0.05) in period II, which offset the increasing trend in period I, resulting in the overall stable pattern. Further investigation was conducted on the variations of surface O_3 during the same periods at nine stations in inland PRD (started from 2006, Table S10). The average O_3 trend in inland PRD showed a remarkable reduction ($p < 0.01$) from 0.74 ± 0.43 ppbv/yr in period I to -0.21 ± 0.52 ppbv/yr in period II (Figure S8), verifying the results above. As discussed in Section 3.1, the alleviation of O_3 pollution over PRD might profit from the change of meteorological conditions. In addition, the substantial reduction of NO_x and VOCs emissions plausibly contributed to the decreased O_3 level over PRD region (Li et al., 2019; Wang et al., 2019b).

Moreover, the variation of regionally-transported O_3 in each season was insignificant ($p > 0.05$), except winter when the regional contribution to O_3 decreased at -0.27 ± 0.11 ppbv/yr, ($p < 0.01$), mainly attributable to the reduction in period II (-0.58 ± 0.28 ppbv/yr, $p < 0.05$). The decline of the regionally-transported O_3 was also discovered in autumn of period II (-1.65 ± 0.36 ppbv/yr, $p < 0.01$), despite an increasing effect of regional O_3 in period I (0.65 ± 0.25 ppbv/yr, $p < 0.01$). As discussed above, the reduced regional effect on O_3 at TC in autumn and winter of period II could be owing to the alleviated O_3 pollution in whole PRD region. Analogous to the impact of meteorological variability on spring O_3 (Section 3.2), the regional influence on O_3 in spring during 2005–2017 was stable ($p = 0.43$), though it increased in period I (0.83 ± 0.19 ppbv/yr, $p < 0.01$), and a steady pattern was found in period II ($p = 0.56$). Again, it was inferred that the increase of spring O_3 during 2005–2017 was mainly caused by local photochemical production, particularly in period II.

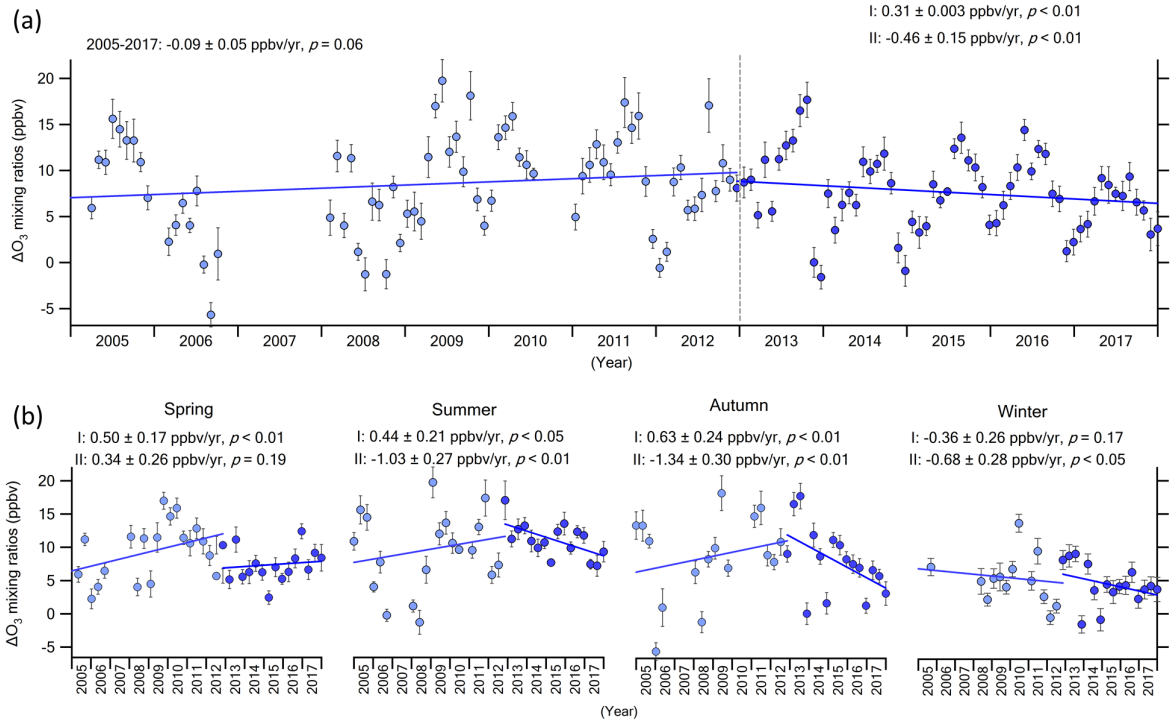

Figure 7. (a) Annual and (b) seasonal variations of regionally-transported O_3 during 2005–2017 (data are integrated into monthly averages, and 95% confidence intervals are given as error bars).

3.3.2 Impacts of O_3 precursors

The variations of locally-produced DM8A O_3 at TC are shown in Figure 8. Overall, an increasing pattern with a rate of 0.29 ± 0.07 ppbv/yr ($p < 0.01$) was observed from 2005 to 2017, suggesting an overall O_3 increase from local photochemical formation. A higher increasing rate (0.49 ± 0.15 ppbv/yr, $p < 0.01$) was found in period I than that in period II (0.18 ± 0.26 ppbv/yr, $p = 0.49$) ($p < 0.01$). The insignificant variation rate in period II suggested that the photochemical oxidative capacity levelled off. Seasonally, the locally-produced O_3 enhanced at a rate of 0.45 ± 0.13 ppbv/yr ($p < 0.01$) in spring. Moreover, locally-produced O_3 increased at rates of 0.68 ± 0.25 ppbv/yr ($p < 0.01$) in period I and 0.72 ± 0.44 ppbv/yr ($p < 0.05$) in period II. Although insignificant variations of locally-produced O_3 were witnessed in summer, autumn and winter ($p > 0.05$), a decrease was discovered in the autumn of period II

548 at a rate of -1.3 ± 0.54 ppbv/yr (p < 0.05), implying significant alleviation of photochemical
549 pollution resulted from reduced local emissions in this period. Similar result was also reported
550 in a previous study in autumn of 2013–2016 (Liu et al., 2019).

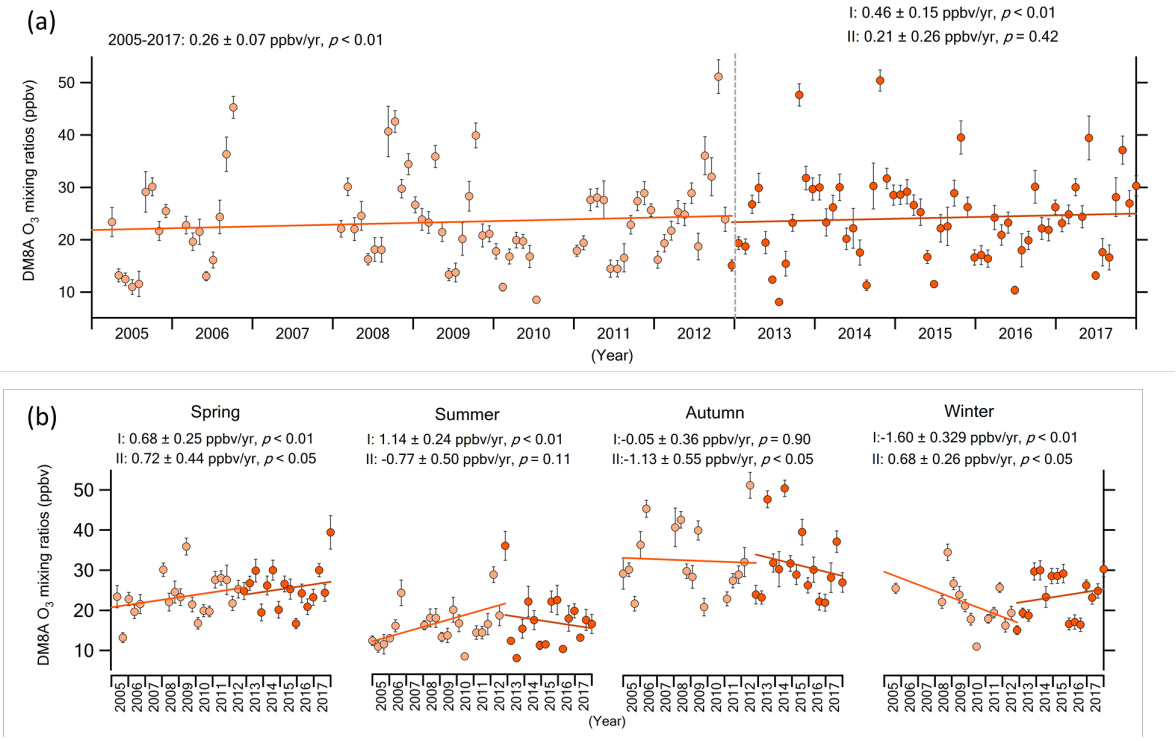

551

552 Figure 8. (a) Annual and (b) seasonal variations of simulated DM8A O_3 during 2005–2017
553 (data is integrated into monthly average at each point, and 95% confidence intervals are shown
554 as error bars).

555 To understand the relationship between O_3 and its precursors, RIR was calculated to identify
556 the changes in sensitivity of O_3 production to its precursors. Figure 9 presents the long-term
557 and seasonal variations of RIR values from 2005 to 2017. In general, TVOC and CO had
558 positive influences on O_3 production, while the negative impact was found for NO_x. Namely,
559 the O_3 formation regime at TC was VOC-limited in all the 13 years. Specifically, the RIR of
560 TVOC increased at a rate of 0.06 ± 0.02 yr^{-1} (p < 0.01), while the RIR of CO decreased at a
561 rate of -0.04 ± 0.02 yr^{-1} (p < 0.05). The results suggested that the sensitivity of O_3 production
562 to TVOC was enhanced, while the sensitivity to CO was decreased. The lessened sensitivity to

CO might be attributed to the decrease of CO concentration (Figure 3). However, the reasons for the increased sensitivity to TVOC are more complex. Although the TVOC concentration remained stable during 2005-2017, other factors such as the variations of speciated VOCs concentrations and VOCs/NO_x ratios could influence the O_3 production sensitivity to TVOC. Besides, the RIR values of NO_x remained stable (p = 0.54), indicating the sensitivity of O_3 production to NO_x has been unchanged during these years.

Similar to the long-term variation of RIR values, positive responses were identified for TVOC and CO while negative effect was found for NO_x in four seasons. The results indicated that the O_3 production was in the VOC-limited regime in each season. It is worth noting that the RIR values of TVOC increased at 0.11 ± 0.05 yr^{-1} (p < 0.01) in spring, suggesting the enhancement of O_3 production sensitivity to TVOC in spring from 2005 to 2017.

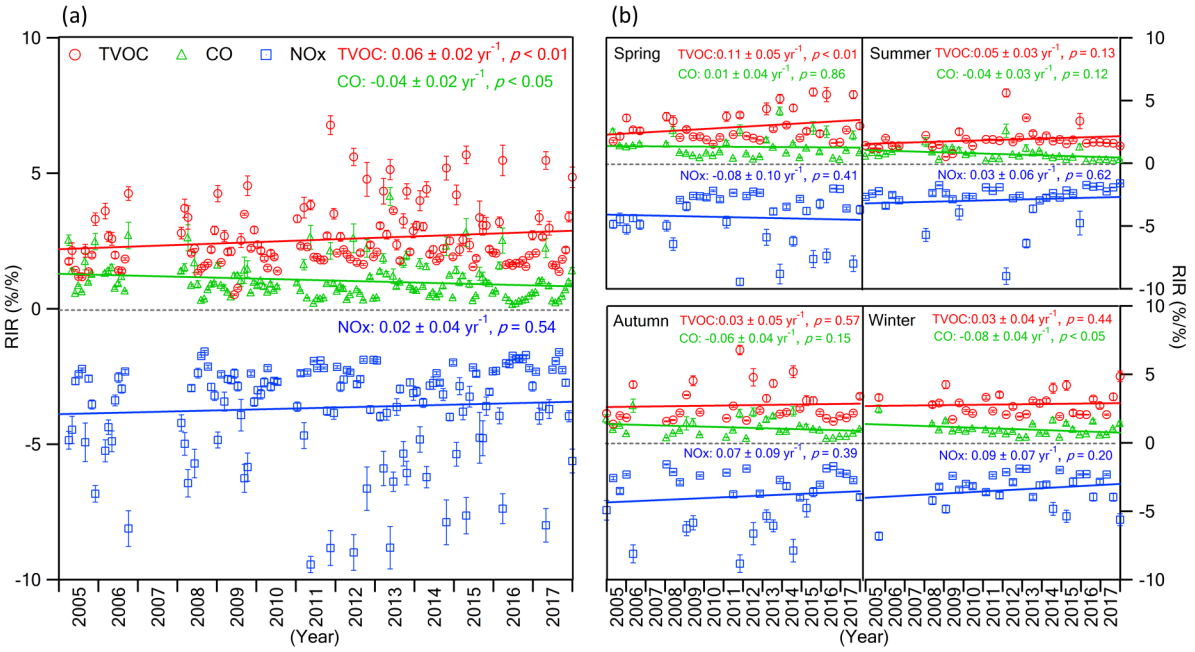

Figure 9. (a) Long-term and (b) seasonal variations of RIR values of O_3 precursors from 2005 to 2017 (the data is based on daytime average (7:00 – 19:00 LST) and integrated into monthly average at each point. 95% confidence intervals are shown as error bars).

578 To further investigate the underlying causes for the long-term variations of in-situ O_3 formation,
579 scenario simulations were conducted with constrained VOCs, NO_x, and CO values (Section
580 2.3). Table S11 lists the O_3 trend of each scenario. Specifically, the overall trend of O_3 from
581 2005 to 2017 significantly ($p < 0.01$. Please note that the p-value here is for the significance
582 test between two data groups) decreased from 0.29 ± 0.07 ppbv/yr ($p < 0.01$) to 0.11 ± 0.09
583 ppbv/yr ($p = 0.21$) with unchanged NO_x set in 2005, implying that local O_3 increased due to
584 NO_x reduction. However, there was no significant difference in the O_3 trends between the base
585 case and the unchanged VOCs scenario ($p = 0.14$), suggesting no impact of TVOC due to its
586 stable pattern during 2005–2017 (Figure 3). The insignificant effect was also found for CO (p
587 = 0.45), possibly due to its low sensitivity to O_3 production (Wang et al., 2017), despite a
588 decline of CO during this period (Figure 3). Same phenomena were observed in the sub-periods,
589 in which the O_3 variation rates insignificantly changed ($p > 0.05$) under the scenario simulations
590 of unchanged VOCs and unchanged CO. However, the locally-produced O_3 pronouncedly
591 decreased ($p < 0.01$) to 0.23 ± 0.19 ppbv/yr ($p = 0.21$) and 0.05 ± 0.23 ppbv/yr ($p = 0.82$) with
592 unchanged NO_x in periods I and II, respectively. Overall, the reduction of NO_x was the main
593 contributor for the long-term increase of locally-produced O_3.

594 Moreover, the seasonal variations of O_3 also verified the critical role of NO_x. When all NO_x
595 concentrations were constrained as the specified value in 2005, the trends of locally-produced
596 O_3 significantly decreased ($p < 0.05$) to -0.07 ± 0.13 ppbv/yr ($p = 0.60$), -0.10 ± 0.09 ppbv/yr
597 ($p = 0.27$), -0.25 ± 0.57 ppbv/yr ($p = 0.29$), and 0.08 ± 0.17 ppbv/yr ($p = 0.65$) in spring, summer,
598 autumn and winter, respectively. It is noteworthy that the remarkable increases of locally-
599 produced O_3 in spring of periods I and II dropped ($p < 0.05$) from 0.68 ± 0.25 ppbv/yr ($p <$
600 0.01) and 0.72 ± 0.44 ppbv/yr ($p < 0.05$) to -0.05 ± 0.27 ppbv/yr ($p = 0.87$) and -0.58 ± 0.44
601 ppbv/yr ($p = 0.06$), respectively. In addition, no significant impact ($p > 0.05$) on the spring O_3
602 trends was identified with the unchanged TVOC and the unchanged CO scenarios. The above

603 results indicated that NO_x reduction was the major culprit for the increased locally-produced
604 O_3 in spring. However, the insignificant difference (p = 0.49) in O_3 trends between the base
605 and the unchanged NO_x scenarios in autumn of period II suggested that NO_x has little
606 contribution to the decrease of autumn O_3, probably attributable to the stable pattern of NO
607 during this period (Figure 4). In contrast, the autumn O_3 trend in period II significantly (p <
608 0.05) shifted from -1.3 ± 0.54 ppbv/yr (p < 0.05) in base scenario to 0.04 ± 0.53 ppbv/yr (p =
609 0.93) in unchanged TVOC scenario, implying that the locally-produced O_3 in autumn of period
610 II was mostly reduced by the decline of TVOC.

611 **4 Conclusions**

612 To investigate the driving forces for the increase of long-term O_3 variation in Hong Kong, this
613 study thoroughly analysed the long-term and seasonal variations of O_3 concentrations from
614 2005 to 2017. The underlying causes were explored from the perspectives of meteorological
615 variability and the components of O_3 budget including physical processes, local
616 photochemistry, based on both statistical calculations and observation-based model. The
617 overall increase of O_3 during 2005–2017 was found, including a rising stage (period I) and a
618 steady stage (period II). The elevated O_3 in period I was attributable to the stimulation of
619 meteorological variability, increase of regional transport, and enhancement of local
620 photochemical production. In contrast, meteorological suppression, decrease of regional
621 transport, and insignificant change of local photochemical production resulted in stable O_3
622 pattern in period II. Seasonally, leveled-off O_3 was observed in autumn during 2005–2017 due
623 to the same reasons as those for long-term variations in period II, which even led to a significant
624 decrease of autumn O_3 in period II as the mitigation of local production. Although the
625 meteorological variability enhanced the O_3 concentrations in summer and winter during 2005–
626 2017, the rise of O_3 in these two seasons have terminated since 2013. However, it was
627 surprisingly found that the continuous NO_x reduction led to the increase in spring O_3 during

2005–2017, particularly the sharp increase in period II, which overwhelmed the decrease of autumn O_3 in the same period. As a consequence, an overall increase of O_3 was observed throughout 2005–2017. In summary, the spring increase prevailed over the hard-earned autumn decrease in O_3 pollution between 2005 and 2017, leading to the increase in the overall O_3 in the past 13 years. Hence, it is of utmost importance to mitigate the increase of spring O_3 to achieve a real drop in overall O_3 in Hong Kong.

Acknowledgments

This study was supported by the Research Grants Council of the Hong Kong Special Administrative Region via Theme-Based Research Scheme (T24-504/17-N) and General Research Fund (PolyU15212421), the Strategic Focus Area Scheme of the Research Institute for Sustainable Urban Development at The Hong Kong Polytechnic University (1-BBW9), the National Key R&D Program of China, Ministry of Science and Technology (No. 2017YFC0212001), and the Hong Kong Polytechnic University PhD scholarships (Project RUJA). The authors thank the Hong Kong Environmental Protection Department for providing air quality monitoring data at Tung Chung site.

References

Agathokleous, E., Feng, Z., Oksanen, E., Sicard, P., Wang, Q., Saitanis, C. J., Araminiene, V., Blande, J. D., Hayes, F., Calatayud, V., Domingos, M., Veresoglou, S. D., Peñuelas, J., Wardle, D. A., Marco, A. D., Li, Z., Harmens, H., Yuan, X., Vitale, M., & Paoletti, E. (2020). Ozone affects plant, insect, and soil microbial communities: A threat to terrestrial ecosystems and biodiversity. *Science Advances*, 6(33), eabc1176. doi:doi:10.1126/sciadv.abc1176

Akimoto, H., Mori, Y., Sasaki, K., Nakanishi, H., Ohizumi, T., & Itano, Y. (2015) Analysis of monitoring data of ground-level ozone in Japan for long-term trend during 1990–2010: Causes of temporal and spatial variation. *Atmospheric Environment*, 102, 302-310, https://doi.org/10.1016/j.atmosenv.2014.12.001.

Appel, K. W., Gilliland, A. B., Sarwar, G., & Gilliam, R. C. (2007). Evaluation of the Community Multiscale Air Quality (CMAQ) model version 4.5: Sensitivities impacting model performance: Part I-Ozone. *Atmospheric Environment*, 41(40), 9603-9615,

https://doi.org/10.1016/j.atmosenv.2007.08.044.

Atkinson, R. (2000). Atmospheric chemistry of VOCs and NO_x. *Atmospheric environment*. 34(12-14), 2063-2101, 4.

Brauer, M., Freedman, G., Frostad, J., van Donkelaar, A., Martin, R. V., Dentener, F., Dingenen, R. v., Estep, K., Amini, H., Apte, J. S., Balakrishnan, K., Barregard, L., Broday, D., Feigin, V., Ghosh, S., Hopke, P. K., Knibbs, L. D., Kokubo, Y., Liu, Y., Ma, S., Morawska, L., Sangrador, J. L. T., Shaddick, G., Anderson, H. R., Vos, T., Forouzanfar, M. H., Burnett, R. T., & Cohen, A. (2016). Ambient Air Pollution Exposure Estimation for the Global Burden of Disease 2013. *Environmental Science & Technology*, 50(1), 79-88. doi:10.1021/acs.est.5b03709.

Chan, C., & Chan, L. (2000). Effect of meteorology and air pollutant transport on ozone episodes at a subtropical coastal Asian city, Hong Kong. *Journal of Geophysical Research: Atmospheres*, 105(D16), 20707-20724. https://doi.org/10.1029/2000JD900140.

Chang, K-L., Petropavlovskikh, I., Cooper, O. R., Schultz, M. G., & Wang, T. (2017). Regional trend analysis of surface ozone observations from monitoring networks in eastern North America, Europe and East Asia. *Elementa: Science of the Anthropocene*, 5: 50, DOI: https://doi.org/10.1525/elementa.243.

Cheng, H. R., Guo, H., Wang, X. M., Saunders, S. M., Lam, S. H., Jiang, F., Wang, T. J., Ding, A. J., Lee, S. C., and Ho, K. F. (2010). On the relationship between ozone and its precursors in the Pearl River Delta: application of an observation-based model (OBM). *Environmental Science and Pollution Research*, 17, 547–560.

Cheng, H. R., Saunders, S. M. Guo, H., Louie, P. K. K., & Jiang, F. (2013). Photochemical trajectory modeling of ozone concentrations in Hong Kong. *Environmental Pollution*, 180, 101-110, doi:https://doi.org/10.1016/j.envpol.2013.04.039.

Collins, W. J., Derwent, R. G., Garnier, B., Johnson, C. E., Sanderson, M. G., & Stevenson, D. S. (2003). Effect of stratosphere troposphere exchange on the future tropospheric ozone trend. *Journal of Geophysical Research*, 108(D12), 8528. https://doi.org/10.1029/2002JD002617.

Cooper, O. R., Forster, C., Parrish, D., Trainer, M., Dunlea, E., Ryerson, T., Hübler, G., Fehsenfeld, F., Nicks, D., Holloway, J., & De Gouw, J. (2004). A case study of transpacific warm conveyor belt transport: Influence of merging airstreams on trace gas import to North America. *Journal of Geophysical Research: Atmospheres.* 109(D23). doi.org/10.1029/2003JD003624.

Cooper, O., Parrish, D., Ziemke, J., Cupeiro, M., Galbally, I., Gilge, S., Horowitz, L., Jensen, N., Lamarque, J., Naik, V., & Oltmans, S. (2014). Global distribution and trends of tropospheric ozone: An observation-based review. *Elementa: Science of the Anthropocene*. doi: 10.12952/journal.elementa.000029.

691 Derwent, R. G., Jenkin, M. E. Saunders, S. M. Pilling, M. J. Simmonds, P. G. Passant, N. R.
692 Dollard, G. Dumitrean, J. P., & Kent, A. (2003), Photochemical ozone formation in north west
693 Europe and its control, *Atmospheric Environment*, 37(14), 1983-1991,
694 doi:https://doi.org/10.1016/S1352-2310(03)00031-1.

695 Derwent, R. G., Jenkin, M. E., & Saunders, S. M. (1996). Photochemical ozone creation
696 potentials for a large number of reactive hydrocarbons under European conditions,
697 *Atmospheric Environment*, 30(2), 181-199, https://doi.org/10.1016/1352-2310(95)00303-G.

698 Ding, A. J., Wang, T., Zhao, M., Wang, T. J., & Li, Z. K. (2004). Simulation of sea-land breezes
699 and a discussion of their implications on the transport of air pollution during a multi-day ozone
700 episode in the Pearl River Delta of China. *Atmospheric Environment*, 38(39), 6737-6750.
701 https://doi.org/10.1016/j.atmosenv.2004.09.017.

702 Feng, S., Jiang, F., Wu, Z., Wang, H., Ju, W., & Wang, H. (2020). CO emissions inferred from
703 surface CO observations over China in December 2013 and 2017. *Journal of Geophysical*
704 *Research: Atmospheres*, 124. https://doi.org/10.1029/2019JD031808.

705 Fishman. J., Wozniak, A. E., & Creilson, J. K. (2003). Global distribution of tropospheric ozone
706 from satellite measurements using the empirically corrected tropospheric ozone residual
707 technique: Identification of the regional aspects of air pollution. *Atmospheric Chemistry and*
708 *Physics*, 3(4):893-907.

709 Gaudel, A., Cooper, O. R., Ancellet, G., Barret, B., Boynard, A., Burrows, J. P., Clerbaux, C.,
710 Coheur, P. F., Cuesta, J., Cuevas, E., Doniki, S., Dufour, G., Ebojie, F., Foret, G., Garcia, O.,
711 Granados-Muñoz, M. J., Hannigan, J. W., Hase, F., Hassler, B., Huang, G., Hurtmans, D., Jaffe,
712 D., Jones, N., Kalabokas, P., Kerridge, B., Kulawik, S., Latter, B., Leblanc, T., Le Flochmoën,
713 E., Lin, W., Liu, J., Liu, X., Mahieu, E., McClure-Begley, A., Neu, J. L., Osman, M., Palm,
714 M., Petetin, H., Petropavlovskikh, I., Querel, R., Rahpoe, N., Rozanov, A., Schultz, M. G.,
715 Schwab, J., Siddans, R., Smale, D., Steinbacher, M., Tanimoto, H., Tarasick, D. W., Thouret,
716 V., Thompson, A. M., Trickl, T., Weatherhead, E., Wespes, C., Worden, H. M., Vigouroux, C.,
717 Xu, X., Zeng, G., & Ziemke, J. (2018). Tropospheric Ozone Assessment Report: Present-day
718 distribution and trends of tropospheric ozone relevant to climate and global atmospheric
719 chemistry model evaluation. *Elementa: Science of the Anthropocene*, 6.
720 doi:10.1525/elementa.291.

721 Georgoulias, A. K.,Van der A, R. J., Stammes, P., Boersma, K. F., & Eskes, H. J. (2019) Trends
722 and trend reversal detection in 2 decades of tropospheric NO_2 satellite observations.
723 *Atmospheric Chemistry and Physics*, 19, 6269–6294, https://doi.org/10.5194/acp-19-6269-
724 2019.

725 Guo, H., So, K. L., Simpson, I. J., Barletta, B., Meinardi, S., & Blake, D. R. (2007). C_1–C_8
726 volatile organic compounds in the atmosphere of Hong Kong: Overview of atmospheric

processing and source apportionment. *Atmospheric Environment*, 41(7), 1456-1472. doi:https://doi.org/10.1016/j.atmosenv.2006.10.011Haman, C. L., Couzo, E., Flynn, J. H., Vizuete, W., Heffron, B., & Lefer, B. L. (2014). Relationship between boundary layer heights and growth rates with ground-level ozone in Houston, Texas. *Journal of Geophysical Research: Atmospheres*, 119(10), 6230-6245. doi:https://doi.org/10.1002/2013JD020473.

He, J., Gong, S., Yu, Y., Yu, L., Wu, L., Mao, H., Song, C., Zhao, S., Liu, H., Li, X., & Li, R. (2017). Air pollution characteristics and their relation to meteorological conditions during 2014–2015 in major Chinese cities. *Environmental Pollution*, 223, 484–496, https://doi.org/10.1016/j.envpol.2017.01.050.

Huang, J. P., Fung, J. C., & Lau, A. K. (2006). Integrated processes analysis and systematic meteorological classification of ozone episodes in Hong Kong. *Journal of Geophysical Research : Atmospheres,* 111(D20), D20309. https://doi.org/10.1029/2005JD007012.

Huang, J. P., Fung, J. C., Lau, A. K., & Qin, Y. (2005). Numerical simulation and process analysis of typhoon-related ozone episodes in Hong Kong. *Journal of Geophysical Research: Atmospheres*, 110(D5), D05301. https://doi.org/10.1029/2004JD004914.

Jiang, F., Guo, H., Wang, T. J., Cheng, H. R., Wang, X. M., Simpson, I. J., Ding, A. J., Sauders, S. M., Lam, S. H. M., & Blake, D. R. (2010). An ozone episode in the Pearl River Delta: Field observation and model simulation. *Journal of Geophysical Research*, 115, D22305. https://doi.org/10.1029/2009JD013583.

Kim, Y., & Lee, G. (2018). Trend of Air Quality in Seoul: Policy and Science. *Aerosol and Air Quality Research*. 18(9):2141-2156.

Lam, Y. F., Cheung, H. M. & Ying, C. C., Impact of tropical cyclone track change on regional air quality. (2018). *Science of the Total Environment*. 610-611, p. 1347-1355.

Lee, Y. C., Shindell, D. T., Faluvegi, G., Wenig, M., Lam, Y. F., Ning, Z., Hao, S., & Lai, C. S. (2014). Increase of ozone concentrations, its temperature sensitivity and the precursor factor in South China. *Tellus B*, 66, 23455, https://doi.org/10.3402/tellusb.v66.23455.

Li, K., Jacob, D. J., Liao, H., Shen, L., Zhang, Q., & Bates, K. H. (2019). Anthropogenic drivers of 2013-2017 trends in summer surface ozone in China. *Proceedings of the National Academy of Sciences*, 116(2):422-427.

Li, M., Liu, H., Geng, G., Hong, C., Liu, F., Song, Y., Tong, D., Zheng, B., Cui, H., Man, H., Zhang, Q., & He, K. (2017). Anthropogenic emission inventories in China: a review. *National Science Review*, 4(6), 834-866. doi:10.1093/nsr/nwx150.

Liao, Z., Ling, Z., Gao, M., Sun, J., Zhao, W., Ma, P., Quan, J., & Fan, S. (2020). Tropospheric ozone variability over Hong Kong based on recent 20-year (2000–2019) ozonesonde

observation. *Journal of Geophysical Research: Atmospheres*, 125, e2020JD033054. https://doi.org/10.1029/2020JD033054.

Lin, C., Li, Y., Lau, A. K. H., Li, C & Fung, J. C. H. (2018). 15-Year $PM_{2.5}$ Trends in the Pearl River Delta Region and Hong Kong from Satellite Observation. *Aerosol and Air Quality Research*, 18: 2355–2362.

Lin, M., Horowitz, L.W., Xie, Y., Paulot, F., Malyshev, S., Shevliakova, E., Finco, A., Gerosa, G., Kubistin, D., & Pilegaard, K. (2020). Vegetation feedbacks during drought exacerbate ozone air pollution extremes in Europe. *Nature Climate Change*, 10, 444–451.

Ling, Z. H., & Guo, H. (2014), Contribution of VOC sources to photochemical ozone formation and its control policy implication in Hong Kong. *Environmental Science & Policy*, 38, 180-191, doi:https://doi.org/10.1016/j.envsci.2013.12.004.

Liu, X., Lyu, X., Wang, Y., Jiang, F., & Guo, H. (2019). Intercomparison of O_3 formation and radical chemistry in the past decade at a suburban site in Hong Kong. *Atmospheric Chemistry and Physics*, 19, 5127–5145, https://doi.org/10.5194/acp-19-5127-2019.

Liu, Y., & Wang, T. (2020a). Worsening urban ozone pollution in China from 2013 to 2017 – Part 2: The effects of emission changes and implications for multi-pollutant control. *Atmospheric Chemistry and Physics*, 20, 6323–6337, https://doi.org/10.5194/acp-20-6323-2020.

Liu, Y., & Wang, T. (2020b). Worsening urban ozone pollution in China from 2013 to 2017 – Part 1: The complex and varying roles of meteorology. *Atmospheric Chemistry and Physics*, 20, 6305–6321, https://doi.org/10.5194/acp-20-6305-2020.

Lu, X., Zhang, L., Wang, X., Gao, M., Li, K., Zhang, Y., Yue, X., & Zhang, Y. (2020). Rapid Increases in Warm-Season Surface Ozone and Resulting Health Impact in China Since 2013. *Environmental Science & Technology Letters*, 7(4), 240-247, DOI: 10.1021/acs.estlett.0c00171.

Luhar, A. K., Galbally, I. E., Woodhouse, M. T., & Thatcher, M. (2017). An improved parameterisation of ozone dry deposition to the ocean and its impact in a global climate–chemistry model. *Atmospheric Chemistry and Physics*, 17(5), 3749-3767.

Lyu, X., Guo, H., Simpson, I. J., Meinardi, S., Louie, P. K. K., Ling, Z., Wang, Y., Liu, M., Luk, C. W. Y., Wang, N., & Blake, D. R. (2016). Effectiveness of replacing catalytic converters in LPG-fueled vehicles in Hong Kong. *Atmospheric Chemistry and Physics*, 16, 6609–6626, https://doi.org/10.5194/acp-16-6609-2016.

Lyu, X., Wang, N., Guo, H., Xue, L., Jiang, F., Zeren, Y., Cheng, H., Cai, Z., Han, L., & Zhou, Y. (2019). Causes of a continuous summertime O_3 pollution event in Jinan, a central city in the North China Plain. *Atmospheric Chemistry and Physics*, 19, 3025–3042, https://doi.org/10.5194/acp-19-3025-2019.

Lyu, X., Zeng, L., Guo, H., Simpson, I., Ling, Z., Wang, Y., Murray, F., Louie, P., Saunders, S., Lam, S., & Blake, D. (2017). Evaluation of the effectiveness of air pollution control measures in Hong Kong. *Environmental Pollution*, 220, 87-94, https://doi.org/10.1016/j.envpol.2016.09.025.

Ma, Z., Xu, J., Quan, W., Zhang, Z., Lin, W., & Xu, X. (2016). Significant increase of surface ozone at a rural site, north of eastern China. *Atmospheric Chemistry and Physics*, 16, 3969–3977, https://doi.org/10.5194/acp-16-3969-2016.

Madronich, S., & Flocke, S. (1997). Theoretical estimation of biologically effective UV radiation at the Earth's surface. In: Zerefos, C. (Ed.), Solar Ultraviolet Radiation-Modeling, Measurements and Effects, NATO ASI Series, vol. I52. Springer-Verlag, Berlin.

Monks, P. S., Archibald, A. T., Colette, A., Cooper, O., Coyle, M., Derwent, R., Fowler, D., Granier, C., Law, K. S., Mills, G. E., Stevenson, D. S., Tarasova, O., Thouret, V., von Schneidemesser, E., Sommariva, R., Wild, O., & Williams, M. L. (2015). Tropospheric ozone and its precursors from the urban to the global scale from air quality to short-lived climate forcer, *Atmospheric Chemistry and Physics*, 15, 8889–8973, https://doi.org/10.5194/acp-15-8889-2015.

Oltmans, S .J., Lefohn, A.S., Harris, J. M., Galbally, I., Scheel, H. E., Bodeker, G., Brunke, E., Claude, H. , Tarasick, D., Johnson, B. J., Simmonds, P., Shadwick, D., Anlauf, K., Hayden, K., Schmidlin, F., Fujimoto, T., Akagi, K., Meyer, C., Nichol, S., Davies, J., Redondas, A., & Cuevas, E. (2006). Long-term changes in tropospheric ozone, *Atmospheric Environment*, 40(17), 3156-3173, https://doi.org/10.1016/j.atmosenv.2006.01.029.

Ou, J. M., Guo, H., Zheng, J. Y., Cheung, K., Louie, P. K. K., Ling, Z. H., & Wang, D. W. (2015). Concentrations and sources of nonmethane hydrocarbons (NMHCs) from 2005 to 2013 in Hong Kong: A multi-year real-time data analysis. *Atmospheric Environment*, 103, 196–206.

Rao, S. T., & Zurbenko, I. G. (1994). Detecting and Tracking Changes in Ozone Air Quality. *Air & Waste*, 44, 1089, https://doi.org/10.1080/10473289.1994.10467303.

Rao, S. T., Zurbenko, I. G., Neagu, R., Porter, P. S., Ku, J. Y., & Henry, R. F. (1997). Space and Time Scales in Ambient Ozone Data. *Bulletin of the American Meteorological Society*, 78, 2153–2166.

Rodgers, J., & Nicewander, W. (1988). Thirteen ways to look at the correlation coefficient. *The American Statistician*, 42(1), 59–66.

Sanchez-Ccoyllo, O. R., Ynoue, R. Y., Martins, L. D., & Andrade, M. D. (2006). Impacts of ozone precursor limitation and meteorological variables on ozone concentration in Sao Paulo, Brazil. *Atmospheric Environment*, 40, 552–562, https://doi.org/10.1016/j.atmosenv.2006.04.069.

Seo, J., Youn, D., Kim, J. Y., & Lee, H. (2014). Extensive spatiotemporal analyses of surface ozone and related meteorological variables in South Korea for the period 1999–2010. *Atmospheric Chemistry and Physics*, 14, 6395–6415, https://doi.org/10.5194/acp-14-6395-2014.

Shindell, D., Faluvegi, G., Nazarenko, L., Bowman, K. Lamarque, J., Voulgarakis, A., Schmidt, G., Pechony, O., & Ruedy, R. (2013). Attribution of historical ozone forcing to anthropogenic emissions. *Nature Climate Change*, 3, 567–570, https://doi.org/10.1038/nclimate1835.

Sicard, P. (2021). Ground-level ozone over time: An observation-based global overview. *Current Opinion in Environmental Science & Health*, 19, 100226. doi:https://doi.org/10.1016/j.coesh.2020.100226

Simon, H., Reff, A., Wells, B., Xing, J., & Frank, N. (2015). Ozone trends across the United States over a period of decreasing NO_x and VOC emissions. *Environmental science & technology*. 49(1):186-195.

Vestreng, V., Ntziachristos, L., Semb, A., Reis, S., Isaksen, I. S. A., & Tarrason, L. (2009). Evolution of NO_x emissions in Europe with focus on road transport control measures. *Atmospheric Chemistry and Physics,* 9, 1503–1520, https://doi.org/10.5194/acp-9-1503-2009.

Vingarzan, R. (2004). A review of surface ozone background levels and trends. *Atmospheric Environment*, 38(21), 3431-3442, https://doi.org/10.1016/j.atmosenv.2004.03.030.

Wang, H., Lyu X. P., Guo, H., Wang, Y., Zou, S. C., Ling, Z. H., Wang, X. M., Jiang, F., Zeren, Y. Z., Pan, W. Z., Huang, X. B., & Shen, J. (2018a). Ozone pollution around a coastal region of South China Sea: interaction between marine and continental air. *Atmospheric Chemistry and Physics*, 18(6), 4277-4295. https://doi.org/10.5194/acp-18-4277-2018.

Wang, K., Zhang, Y., Yahya, K., Wu, S., & Grell, G. (2015). Implementation and initial application of new chemistry-aerosol options in WRF/Chem for simulating secondary organic aerosols and aerosol indirect effects for regional air quality. *Atmospheric Environment*, 115, 716-732, , https://doi.org/10.1016/j.atmosenv.2014.12.007m.

Wang, T., Dai, J., Se Lam, K., Poon, C. N., & Brasseur, G. P. (2019a). Twenty-Five years of lower tropospheric ozone observations in tropical East Asia: The influence of emissions and weather patterns. *Geophysical Research Letters*, 46(20), 11463–11470, https://doi.org/10.1029/2019GL084459.

Wang, N., Lyu, X., Deng, X., Huang, X., Jiang, F., & Ding, A. (2019b). Aggravating O_3 pollution due to NO_x emission control in eastern China. *Science of The Total Environment*, 677, 732-744, https://doi.org/10.1016/j.scitotenv.2019.04.388.

Wang, Y., Wang, H., Guo, H., Lyu, X., Cheng, H., Ling, Z., Louie, P. K. K., Simpson, I. J., Meinardi, S., & Blake, D. R. (2017). Long-term O_3–precursor relationships in Hong Kong:

field observation and model simulation. *Atmospheric Chemistry and Physics*, 17, 10919–10935, https://doi.org/10.5194/acp-17-10919-2017.

Wang, Y., Guo, H., Zou, S. C., Lyu, X. P., Ling, Z. H., Cheng, H. R., & Zeren, Y. Z. (2018b). Surface O_3 photochemistry over the South China Sea: Application of a near□explicit chemical mechanism box model. *Environmental Pollution*, 234, 155–166.

Willmott, C. J. (1981). On the validation of models. *Physical Geography*, 2(2), 184–194.

World Health Organization (WHO). (2003). Regional Office for Europe.: Health aspects of air pollution with particulate matter, ozone and nitrogen dioxide: report on a WHO working group, Bonn, Germany 13-15 January 2003. Copenhagen: WHO Regional Office for Europe. http://www.who.int/iris/handle/10665/107478.

Xu, J., Tie, X., Gao, W., Lin, Y., & Fu, Q. (2019). Measurement and model analyses of the ozone variation during 2006 to 2015 and its response to emission change in megacity Shanghai, China. *Atmospheric Chemistry and Physics*, 19, 9017–9035, https://doi.org/10.5194/acp-19-9017-2019.

Xue, L., Ding, A., Cooper, O., Huang, X., Wang, W., Zhou, D., et al. (2020). ENSO and Southeast Asian biomass burning modulate subtropical trans-Pacific ozone transport. *National Science Review.* https://doi.org/10.1093/nsr/nwaa132

Xue, L. K., Wang, T., Louie, P. K., Luk, C. W., Blake, D. R., & Xu, Z. (2014). Increasing external effects negate local efforts to control ozone air pollution: a case study of Hong Kong and implications for other Chinese cities. *Environmental science & technology*, 48, 10769–10775, https://doi.org/10.1021/es503278g.

Yan, Y., Pozzer, A., Ojha, N., Lin, J., & Lelieveld, J. (2018). Analysis of European ozone trends in the period 1995–2014. *Atmospheric Chemistry and Physics*, 18(8), 5589-5605. doi:10.5194/acp-18-5589-2018.

Yang, L., Luo, H., Yuan, Z., Zheng, J., Huang, Z., Li, C., Lin, X., Louie, P. K. K., Chen, D., & Bian, Y. (2019). Quantitative impacts of meteorology and precursor emission changes on the long-term trend of ambient ozone over the Pearl River Delta, China, and implications for ozone control strategy. *Atmospheric Chemistry and Physics*, 19, 12901–12916, https://doi.org/10.5194/acp-19-12901-2019.

Yang, Y., Shao, M., Wang, X., Nölscher, A. C., Kessel, S., Guenther, A., & Williams, J. (2016). Towards a quantitative understanding of total OH reactivity: A review. *Atmospheric Environment*, 134, 147-161. doi:https://doi.org/10.1016/j.atmosenv.2016.03.010

Yarwood, G., Rao, S., Yocke, M., & Whitten, G. (2005). Updates to the carbon bond chemical mechanism: CB05. Final report to the U.S. EPA, RT-0400675,

http://www.camx.com/publ/pdfs/cb05_final_report_120805.pdf.

Young, P. J., Archibald, A. T., Bowman, K. W., Lamarque, J.-F., Naik, V., Stevenson, D. S., Tilmes, S., Voulgarakis, A., Wild, O., Bergmann, D., Cameron-Smith, P., Cionni, I., Collins,W. J., Dalsøren, S. B., Doherty, R. M., Eyring, V., Faluvegi, G., Horowitz, L. W., Josse, B., Lee, Y. H., MacKenzie, I. A., Nagashima, T., Plummer, D. A., Righi, M., Rumbold, S. T., Skeie, R. B., Shindell, D. T., Strode, S. A., Sudo, K., Szopa, S., & Zeng, G. (2013). Preindustrial to end 21st century projections of tropospheric ozone from the Atmospheric Chemistry and Climate Model Intercomparison Project (ACCMIP). *Atmospheric Chemistry and Physics*, 13, 2063–2090, doi:10.5194/acp-13-2063-2013.

Zeren, Y., Guo, H., Lyu, X., Jiang, F., Wang, Y., Liu, X., Zeng, L., Li, M., & Li, L. (2019). An ozone "pool" in South China: Investigations on atmospheric dynamics and photochemical processes over the Pearl River Estuary. *Journal of Geophysical Research: Atmospheres*, 124. https://doi.org/10.1029/2019JD030833.

Zhang, L., Brook, J. R., & Vet, R. (2003). A revised parameterization for gaseous dry deposition in air‐quality models. *Atmospheric Chemistry and Physics*, 3, 2067–2082.

Zhang, Y. & Dubey, M. K. (2009). Comparisons of WRF/Chem simulated O_3 concentrations in Mexico City with ground-based RAMA measurements during the MILAGRO period. *Atmospheric Environment*, 43(30), 4622-4631.

Zheng, B., Tong, D., Li, M., Liu, F., Hong, C., Geng, G., Li, H., Li, X., Peng, L., Qi, J., & Yan, L., (2018). Trends in China's anthropogenic emissions since 2010 as the consequence of clean air actions. *Atmospheric Chemistry and Physics*. 18(19):14095-14111, https://doi.org/10.5194/acp-18-14.

Zheng, J., Shao, M., Che, W., Zhang, L., Zhong, L., Zhang, Y., & Streets, D. (2009). Speciated VOC emission inventory and spatial patterns of ozone formation potential in the Pearl River Delta, China. *Environmental Science & Technology*, 43(22), 8580-8586. doi:10.1021/es901688e.